# Nonlinear, Non-Stationary Analysis of Interarea Oscillations via Hilbert Spectral Analysis

A. R. Messina, *Senior Member, IEEE*, and Vijay Vittal, *Fellow, IEEE*

***Abstract*—Hilbert spectral analysis (HSA) is used to characterize the time evolution of non-stationary power system oscillations following large perturbations. Using an analytical procedure based on the Hilbert–Huang Technique (HHT), data from transient stability simulations are decomposed into a finite number of time-varying oscillating components that can be associated with different time scales. Hilbert analysis is then utilized to characterize the time evolution of critical components giving rise to the observed oscillations. The objectives of this study are to obtain information of a quantitative nature on nonlinear processes in power system oscillatory phenomena and assess the applicability of the developed procedures to track the evolving dynamics of critical system modes.**

**A six-area, 377-machine power system is analyzed to examine the onset of nonlinear, non-stationary behavior. Examples of the developed procedures to detect and quantify the strength of nonlinear interaction in power system behavior and to estimate the distribution of the non-stationarity are provided.**

***Index Terms*—Nonlinear systems, power system dynamic stability, spectral analysis.**

## I. Introduction

THE STUDY of nonlinear, non-stationary power system oscillations has recently become the subject of intense interest and investigation in power system stability studies [1]–[4]. Detailed results, however, have generally been limited to the case of semi-stationary processes in simple power systems.

Proper understanding of the dynamics of these oscillations requires investigation of the various types of temporal nonlinear interactions involving the fundamental modes of the system [2], [4]. The detection and characterization of temporal oscillations in simulated data is greatly complicated by non-stationary variations in system dynamic behavior. Detection of nonstationarities enables the determination of the length of data records needed to provide better estimates of the dynamical spectra and the selection of the most appropriate techniques to track changes in the system.

In addition, characterization of the temporal variation of the fundamental modes of oscillation may facilitate the effective control of the system.

Recent analytical investigations into the nonlinear dynamics of complex systems have documented and predicted the existence of nonlinear interaction among the inertial modes of the system [2]–[5]. In a previous paper [2], the authors used higher-order statistical (HOS) techniques to study the interplay of modal interaction and nonlinear behavior in a complex system. HOS methods, however, are mainly useful for the analysis of semi-stationary phenomena whose frequency components change slowly over time.

Several representations have been explored over the last few years to analyze processes that are characterized by nonlinear, non-stationary characteristics. In [3] and [4], Hilbert spectral analysis (HSA) and normal form theory were used to predict the onset of nonlinear behavior arising from the interaction between the electromechanical modes of the system. In [5], time series analyses techniques were applied to analyze measured data from non-stationary power system oscillations. Although these studies have lead to significant advances in the understanding of system dynamics, to date, no systematic studies to extract accurate information on the nature of system temporal behavior have been proposed.

In this paper, we extend the HSA approach proposed by [3] to detect and quantify the effect of nonlinear mode interaction in the time evolution of non-stationary interarea oscillations. Using an analytical procedure based on the HHT, the simulated data are decomposed into a finite number of time-varying oscillating components that can be associated with different time scales. HSA is then utilized to determine temporal characteristics of the underlying modal components.

The use of the analysis techniques is tested on a six-area, 377-machine practical power system. Comparison of numerical results using HSA to conventional approaches confirms the accuracy of the developed procedures.

## II. Outline of the Study

The system under investigation is a six-area, 377-machine detailed model of the Mexican interconnected power system used by the authors in a previous study [2]. Fig. 1 depicts the general structure of this system showing the main areas of concern for this study. This model has been correlated with small and large performance simulation results, and a good agreement between both approaches has been found.

### A. Test Cases and System Operating Conditions

The weak nature of interconnections in the study system poses a limit to power transfers between areas and is a major cause of the onset of low-frequency oscillations. Numerical simulations of several contingency scenarios were used to investigate the onset of nonlinear and non-stationary characteristics.

Two contingency scenarios are selected to infer the strengths of nonlinear interactions [2].

**Case A**. Outage of Laguna Verde (LGV) unit #1. This case assumes the outage without fault of unit #1 (650 MW) of

Manuscript received May 11, 2005; revised January 4, 2006. Paper no. TPWRS-00236-2005.

A. R. Messina is with the Department of Electrical Engineering, Arizona State University, Tempe, AZ 85287-5706 USA, on leave from Cinvestav, Mexico City, Mexico (e-mail: aroman@gdl.cinvestav.mx).

V. Vittal is with the Department of Electrical Engineering, Arizona State University, Tempe, AZ 85287-5706 USA (e-mail: vijay.vittal@asu.edu).

Digital Object Identifier 10.1109/TPWRS.2006.876656

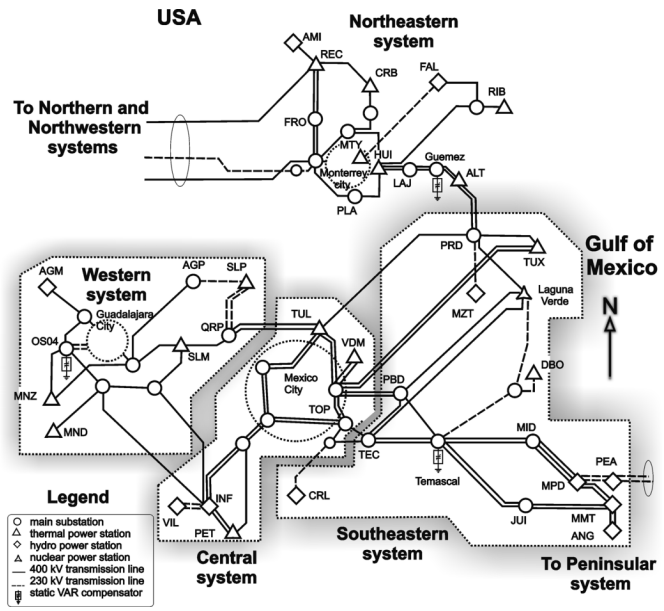


Fig. 1. Geographical schematic of the areas of interest.

the Laguna Verde (LGV) nuclear power station, one of the two largest units in the system, in the southeastern network of the system.

**Case B**. Simultaneous outage of critical transmission paths. This simulation assumes the simultaneous line outage without fault of one circuit of the 400-kV line from MMT to JUI and the 400-kV line from Temascal (TMD) to PBD on the 400-kV network of the southeastern system.

For both cases, it is assumed that PSSs and supplementary damping controllers are removed from operation to enable the detailed study of the role of modal interaction in the onset of system instability.

The analysis of case A is of particular importance since it causes destabilization of critical system modes and, without remedial control measures, results in uncontrolled system separation, involving nonlinear quadratic coupling resulting from nonlinear interaction of the slowest modes of the system. Case B, in turn, provides a unique opportunity to study the interplay between nonlinear modal interaction and temporal fluctuations in the observed system response.

TABLE I
EIGENVALUES OF THE SYSTEM FOR THE POST-CONTINGENCY CONDITION

| Mode description | Case A | Case B |
|---|---|---|
| Inter-area mode 1 | 0.025±j1.828 (0.29 Hz, ζ=-1.37%) | -0.011±j2.010 (0.31 Hz, ζ=0.57%) |
| Inter-area mode 2 | 0.037±j3.245 (0.52 Hz, ζ=-1.13%) | -0.032±j3.251 (0.51 Hz, ζ=0.98%) |
| Inter-area mode 3 | -0.047±j3.906 (0.62 Hz, ζ=1.20%) | -0.043±j3.912 (0.62 Hz, ζ=1.09%) |
| Inter-area mode 4 | 0.015±j4.854 (0.77 Hz, ζ=-0.31%) | -0.031±j4.824 (0.76 Hz, ζ=0.64%) |
| Mode 5 | -0.196±j5.698 (0.92 Hz, ζ=3.44%) | -0.177±j5.693 (0.91 Hz, ζ=3.10%) |

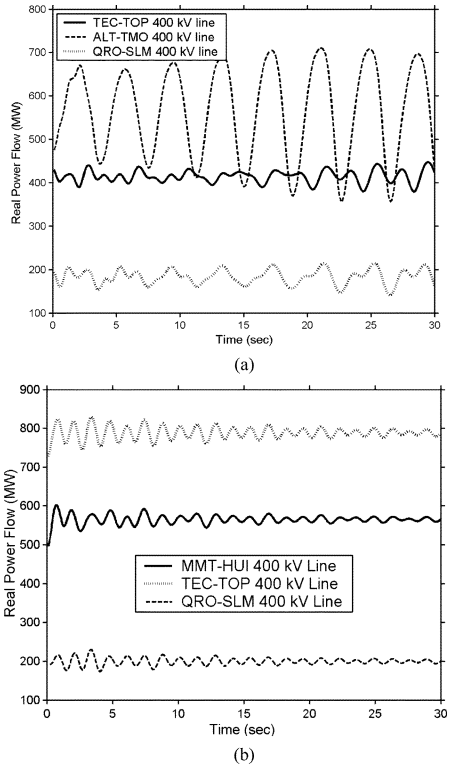


Fig. 2. System response to critical contingencies. (a) Case A. (b) Case B.

### *B. Damping Characteristics in the Study System*

Modal analysis performed for the post-contingency condition has identified three critical interarea modes associated with the interaction of machines in the north and south systems.

- Two critical interarea modes at 0.32 and 0.52 Hz representing the interaction of machines in the north and south systems and the east and central and west systems, respectively.
- Three higher frequency modes at 0.62, 0.77, and 0.92 Hz representing localized interaction of machines in the north and south systems.

Table I gives the slowest eigenvalues of the system for the post-contingency conditions above. Results from previous work indicate that nonlinear interactions between these modes can occur, leading to a complex system dynamic behavior especially under heavy stress conditions [2], [5].

These interactions play an important role in the small and large system response and may contribute significantly to the time evolution of the observed oscillations as discussed below.

### *C. Dynamic Response to Large Perturbations*

Selected simulation results for cases A and B are shown in Fig. 2. The nature of these oscillations becomes evident from the analysis of the power spectra of selected signals in Fig. 3. For case A, outage of Laguna Verde unit #1 is seen to excite the 0.29-Hz interarea mode 1 and the 0.52-Hz interarea mode 2 on the transmission lines in the north systems (namely, ALT-TMO), and the interarea modes 1, 2, 4, and 5 on the 400-kV

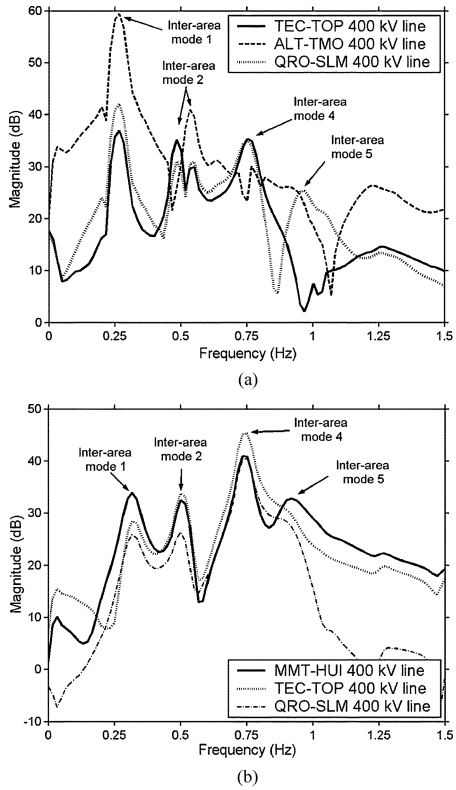


Fig. 3. Fourier spectra of active power flows for cases A and B. (a) Case A. (b) Case B.

networks of the southeastern (TEC-TOP) and western interconnections (QRO-SLM).

For case B, the analysis of the linear spectra for interconnections in the western and southeastern networks in Fig. 3(b) shows the presence of the 0.76-Hz interarea mode 4, the 0.92-Hz interarea mode 5, the 0.51-Hz interarea mode 2, and the 0.32-Hz interarea mode 1.

Common characteristics of the observed oscillations include the presence of multiple dominant modes and nonlinear interaction of quadratic and cubic nature between the primary modes of the system.

The dynamic data obtained from these simulations are used for HSA in the following sections.

## III. Hilbert Spectral Analysis

### A. Background—The Empirical Mode Decomposition (EMD)

The EMD method is a technique to decompose an arbitrary signal $x(t)$, into a number of Intrinsic Mode Function (IMF) components with time variable amplitudes and frequencies [6].

This decomposition can be represented mathematically by $x(t) = \sum_{j=1}^{n} c_j(t) + r_n(t)$, where $c_j(t)$ is the $j$th IMF, $n$ is the number of IMFs, and $r_n(t)$ is the residue. Each IMF represents a simple time-varying oscillatory mode with different amplitude and frequency content and can have both amplitude and frequency modulation. By construction, IMFs are nearly orthogonal: the first IMF captures the highest frequency content; the frequency content decreases with the increase in IMF. Details of this procedure are given in [1] and [3].

Based upon this discussion, we rewrite the above decomposition in the form

$$x(t) = \sum_{j=1}^{n} x_j(t) + r_n(t) = \sum_{j=1}^{p} c_j(t) + \sum_{k=p+1}^{n} c_k(t) + r_n(t) \tag{1}$$

where the terms $c_j(t)$, $j = 1, \ldots, p$ contain the physical behavior of interest, and the remaining $n - p$ terms contain uninteresting, non-sinusoidal characteristics.

The Hilbert transform is then applied to the IMF components to determine the Hilbert spectrum.

### B. Hilbert Spectral Analysis

Application of the Hilbert transformation to (1) yields

$$z(t) \approx \sum_{j=1}^{p} x_j(t) + i x_{Hj}(t) = \sum_{j=1}^{p} A_j(t) e^{i\varphi_j(t)} = A(t) e^{i\varphi(t)} \tag{2}$$

where $x_{Hj}(t)$ is the Hilbert transform of $c_j(t)$, $A_j(t) = \sqrt{x_j(t)^2 + x_{Hj}(t)^2}$, and $\varphi_j(t) = \arctan(x_{Hj}(t)/x_j(t))$.

From (2), we obtain

$$\dot{z}(t) \approx \sum_{j=1}^{p} A_j(t) e^{i\varphi_1(t)} \left(i\omega_j(t)\right) + \sum_{j=1}^{p} e^{i\varphi_1(t)} \dot{A}_j(t) \tag{3}$$

where $\omega_j(t) = d\varphi_j(t)/dt$ is the instantaneous frequency. Combining (2) and (3) gives

$$\frac{\dot{z}(t)}{z(t)} = \left[\frac{\dot{A}(t)}{A(t)} + i\omega(t)\right] \tag{4}$$

from which it follows that $\omega(t) = \mathrm{Im}[\dot{z}(t)/z(t)]$. The same analysis is valid for the $j$th mode complex signal $\dot{z}_j(t)/z_j(t)$, where $z_j(t) = x_j(t) + i x_{Hj}(t)$. The original signal can then be expressed as the real part of the complex expansion

$$\hat{x}(t, A, \omega) \approx \mathrm{Re}\left[\sum_{j=1}^{p} A_j(t) e^{i\int_o^t \omega_j(t)dt}\right] \tag{5}$$

which defines a generalized form of the Fourier spectra with time-varying amplitudes and phases designated as the Hilbert spectrum. If $p = n$, (5) reproduces $x(t) - r_n(t)$, exactly.

### C. Damping Characterization

In the procedures developed in this paper, a more useful alternative to the analysis of local behavior is obtained by assuming that $A_j(t) = \Lambda_j(t)\exp(\eta_j(t))$ [7], where $\eta_j(t) = -\int_o^t \alpha_j(t)dt)$ is an exponential factor characterizing the time-dependent decay of the waves for the $j$th component, and $\alpha_j(t)$ is the associated instantaneous damping.

Use of this assumption in (2) and (3) results in

$$\frac{\dot{z}_j(t)}{z_j(t)} = \left[\left(-\alpha_j(t) + \frac{\dot{\Lambda}_j(t)}{\Lambda_j(t)}\right) + i\omega_j(t)\right]. \tag{6}$$

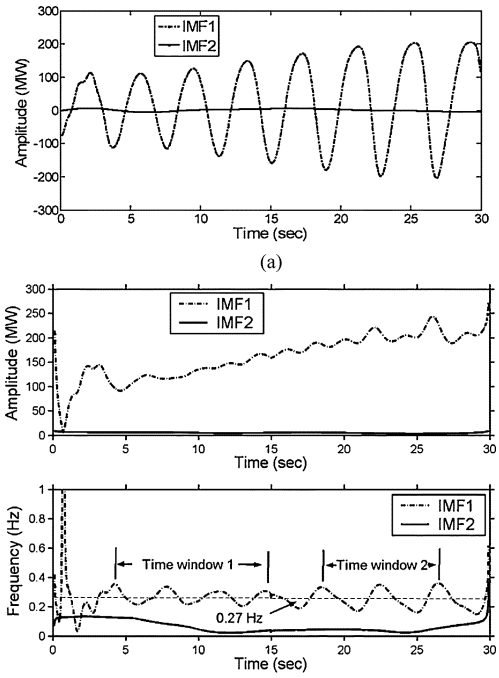


Fig. 4. Hilbert spectral analysis of the ALT-TMO power signal. Case A. (a) Intrinsic mode functions. (b) Instantaneous characteristics.

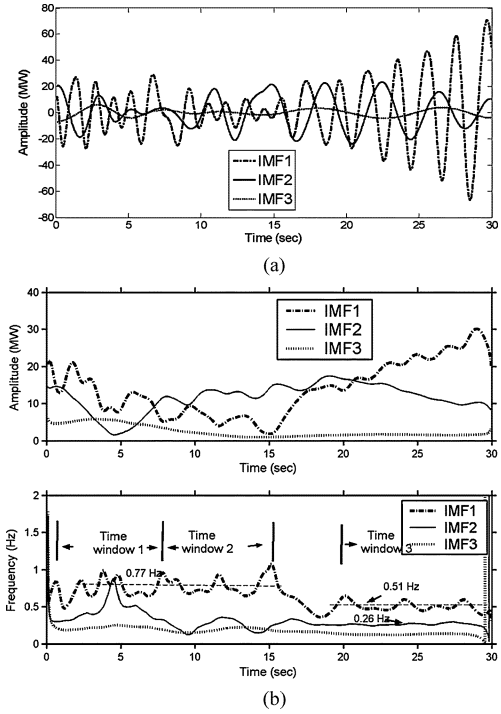


Fig. 5. Hilbert spectral analysis of the TEC-TOP power signal. Case A. (a) Intrinsic mode functions. (b) Instantaneous amplitude and frequency.

Noting that $\mathrm{Re}[\dot{z}_j(t)/z_j(t)] = \dot{A}_j(t)/A_j(t)$ [8], we get

$$\alpha_j(t) = -\frac{d\eta_j(t)}{dt} = -\left\{\frac{\dot{A}_j(t)}{A_j(t)} - \frac{\dot{\Lambda}_j(t)}{\Lambda_j(t)}\right\}, \quad j = 1, \ldots p \tag{7}$$

where $[\dot{A}_j(t)/A_j(t)] = (x_j(t)\dot{x}_j(t) + x_{Hj}(t) + \dot{x}_{Hj}(t))/A_j^2(t)$. With this approach, it becomes possible to estimate the local damping associated with each local time scale of the data.

### D. Case A

Figs. 4–6 show the IMF components for selected signals extracted following the procedure in [3]. To permit comparison with the results of other analysis techniques in Section III-F, the data were divided into several segments exhibiting nearly stationary behavior.

For the ALT-TMO 400-kV line, application of the EMD technique for case A in Fig. 4(a) identifies, essentially, a dominant IMF centered at about 0.27 Hz disclosing the presence of inter-area mode 1. Visual inspection of the instantaneous frequency in Fig. 4(b) suggests intra-wave modulation in which a second mode modulates the 0.27-Hz mode to produce a response in the Hilbert spectrum whose frequency slowly varies with time.[1] For time window 1, the degree of modulation is very small, indicating an essentially mono-component behavior.

As time progresses, however, frequency modulation increases. This is an important observation since the analysis suggests that as the system approaches instability, two or more modes of differing time scales make a significant contribution

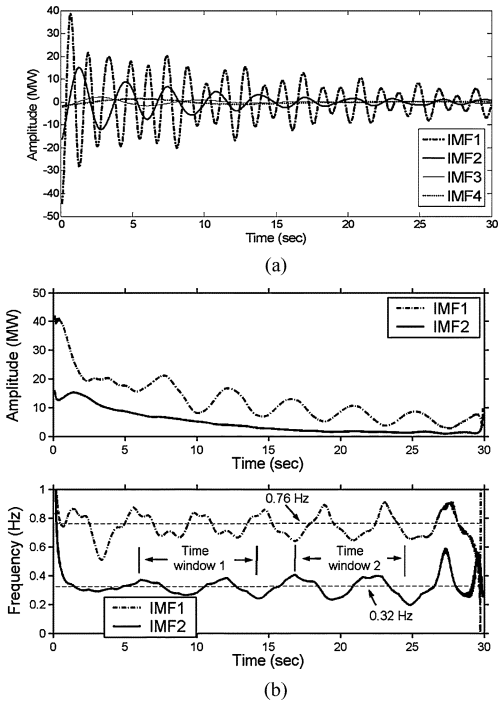


Fig. 6. Instantaneous attributes of MMT-JUI real power flow. Case B. (a) Intrinsic mode functions. (b) Instantaneous amplitude and frequency.

[1]Assuming $z(t) = [A_1(t)\exp(i\varphi_1(t)) + A_2(t)\exp(i\varphi_2(t))]$ and neglecting fast transients in $A_j(t)$ in (3), the instantaneous frequency $w(t)$ can be expressed as

$$\omega(t) = \omega_1(t) + \left[\frac{A_2^2 + A_1(t)A_2(t)\cos(\phi_2(t) - \phi_1(t))}{A^2(t)}\right] \times (\omega_2(t) - \omega_1(t))$$

This defines a nonlinear and non-stationary frequency (amplitude)-modulated signal. Analogous expressions hold for third-order interactions and form the basis for the study of higher order interaction in later sections.

to the observed oscillation; this also suggests that time-synchronized control action on these modes might be used to more effectively stabilize the system.

For the 400-kV line, TEC-TOP examination of the modal components in Fig. 5 identifies three distinct stages in which several IMFs make a significant contribution to system response. HSA in Fig. 5(b) shows the presence of a higher frequency mode at about 0.77 Hz, a low-frequency mode at 0.51 Hz, and two essentially stationary modes at 0.26 and 0.12 Hz. For time windows 1 and 2, the frequency of IMF1 oscillates around 0.77 Hz to then decrease in time to about 0.51 Hz near the end of time window 2. The remainder of the signal still exhibits frequency-modulated oscillations but of a much smaller amplitude with a steady-state value of about 0.51 Hz. Examination of IMF2, in turn, shows a transition from a 0.51 Hz mode in time window 1 to a nearly stationary mode at about 0.26 Hz for window 3. In addition, a third subharmonic oscillation at about 0.12 Hz is also noticeable in the time evolution of IMF3. This latter mode shows a less variable behavior, but its effect disappears rapidly, as indicated by the decaying amplitude in Fig. 5(a).

The analysis of instantaneous amplitudes of the IMFs in Fig. 5(a) provides further insight into the nature of the oscillations. The temporal evolution of these components is very complex. In the initial stage, i.e., $t \leq 15\ s$, the amplitude of IMF1 decreases while that of IMF2 decreases for $t \leq 5\ s$ to then increase almost monotonically. At the end of this initial stage at about 15 s, the amplitude of IMF1 gradually increases in magnitude indicating unstable behavior. The fluctuation of frequency with amplitude of this mode is an indicator of nonlinear effects in the mechanism causing the oscillation.

### *E. Case Study B*

Fig. 6 shows HSA results for the MMT-JUI signal. Application of the EMD method to the MMT-JUI signal in Fig. 6(a) results in four nonstationary modes. IMFs 1 and 2 appear to capture the relevant information. Of practical interest, oscillations in IMFs 1 and 2 with frequencies centered around 0.76 and 0.32 Hz are seen to persist for approximately 30 s. The amplitude of these oscillations decreases with time, revealing an essentially stable behavior.

The temporal behavior of IMFs 1 and 2 for the MMT-JUI signal in Fig. 6(b) suggests again the presence of strong frequency modulation in which the amplitude of the frequency oscillations increases in time. The interaction becomes strong as time progresses, as suggested by the increasing frequency variations, thus emphasizing the need for simultaneous control of the interacting modes.

In order to independently confirm the results demonstrated by Hilbert analysis, we selected the ALT-TMO, TEC-TOP, and MMT-JUI signals and examined the effects of mode interactions in the system response using HOS techniques. These were then compared with those obtained using conventional spectral analysis.

### *F. Comparison With Spectral Analyses*

To aid in the interpretation of Hilbert results, the data were processed using the selected windows. Such an approach provides some insight into the time-varying nature of the spectral dynamics. Figs. 7–9 show the evolution of the spectra for selected signals. With prior knowledge of the time scales involved in the dynamics, the Fourier spectra is able to detect the nature of temporal-space behavior.

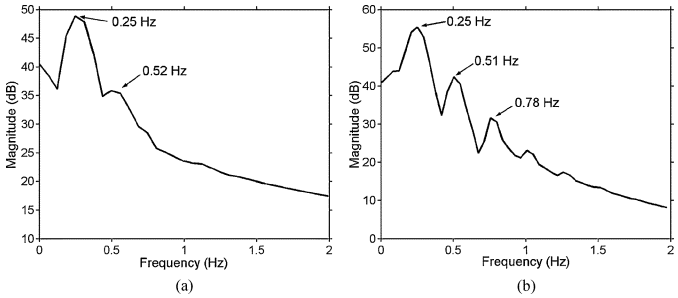


Fig. 7. Windowed Fourier spectra of IMF1 of the ALT-TMO signal. Case A. (a) Time window 1. (b) Time window 2.

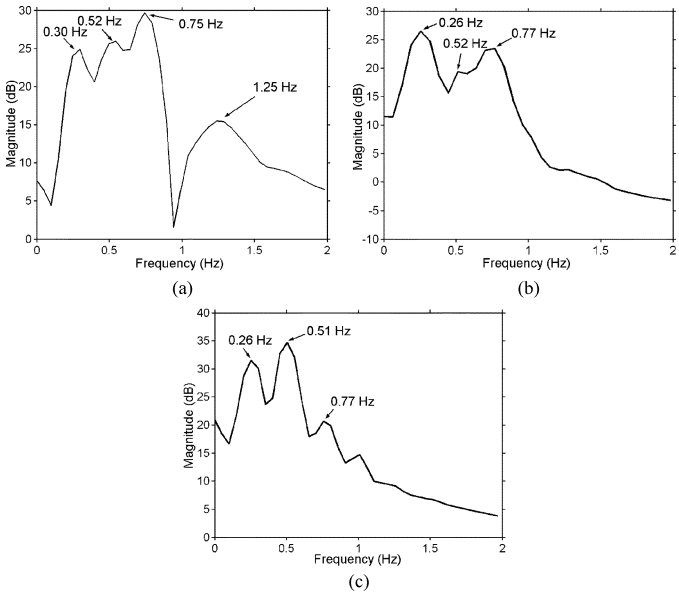


Fig. 8. Windowed Fourier spectra of IMF1 of the TEC-TOP signal. Case A. (a) Time window 1. (b) Time window 2. (c) Time window 3.

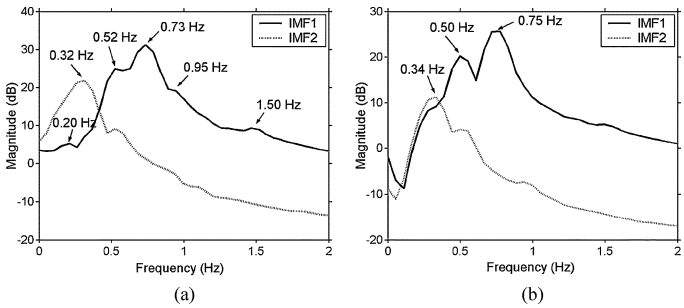


Fig. 9. Windowed spectra of IMFs 1 and 2 of the MMT-JUI signal. Case B. (a) Time window 1. (b) Time window 2.

For the ALT-TMO signal, the analysis of time window 1 in Fig. 7(a) shows essentially a dominant peak at about 0.25 Hz, thus confirming the presence of interarea mode 1. It is interesting to note that, as time evolves, the degree of frequency modulation increases.

Components at 0.25, 0.51, and 0.78 Hz in Fig. 7(b) show evidence of nonlinear modal interaction in which the sum frequency of modes 1 and 2 is equal to that of mode 4 at 0.75 Hz. This is clearly demonstrated in Fig. 4(b) that shows increased modulation activity in window 2.

Simulation results for the TEC-TOP signal in Fig. 8 provide further insight into the nature of dynamic behavior. A comparison of the power spectra for the TEC-TOP signal in Fig. 8 and the time evolution of the instantaneous frequency in Fig. 5(b) shows that HSA accurately tracks the evolving dynamics of the critical modes.

For time window 1, the spectra shows the interaction of interarea modes 1, 2, and 4. A higher frequency mode at 1.25 Hz is also observed. Most likely, this is the result of nonlinear coupling between the 0.75-Hz mode and the 0.52-Hz mode to yield the 1.25-Hz component. For time window 2, the dominant modes are interarea modes 1 and 4. Finally, the analysis of time window 3 shows the dominant participation of modes 1 and 2. This agreement is found to be quite satisfactory with HSA in Fig. 5(b).

In turn, analysis of the MMT-JUI signal in Fig. 9 shows the participation of modes 1, 2, 4, and 5. As seen from this figure, IMF1 is seen to capture the nonlinear interaction between the 0.75- and the 0.52-Hz modes, whereas IMF2 captures the interaction between the 0.32- and the 0.52-Hz modes. For time window 1, the Fourier spectra in Fig. 9(a) shows dominant peaks at 0.73, 0.32, and 0.52 Hz. The analysis also suggests that nonlinear interaction of these modes gives rise to secondary oscillations at about 0.20 Hz formed by the difference frequency of the 0.52- and the 0.32-Hz modes. In addition, a second harmonic of the 0.73-Hz mode is observed.

Comparison of the spectrum for time window 2 with that of window 1 also indicates that the presence of the 0.52-Hz interarea mode 2 relative to the 0.75-Hz mode 4 increases. This demonstrates an increase in the degree of frequency modulation of the 0.32-Hz interarea mode 1 and the 0.76-Hz interarea mode 4 as suggested by the Hilbert spectra in Fig. 6(b).

In an attempt to better quantify nonlinear effects in the observed behavior and confirm the results of the previous analysis, HOS was applied to the time series.

To estimate higher-order spectra for the record $x(k)$, the time series was divided into several equal overlapping segments, and the bispectrum $B(\omega_1,\omega_2)$[2] was estimated using an ARMA model [2]. The trispectrum $T(\omega_1,\omega_2,\omega_3)$ was then used to detect four-wave interactions and cubic phase coupling.

Figs. 10 and 11 show a contour plot of the parametric estimates of the magnitude of the bispectrum, as a function of the interacting frequencies for the TEC-TOP and the MMT-HUI signals. The analysis is confined to the part of physical interest of the spectrum $(f_1, f_2 < 1\text{Hz})$. Further, a two-dimensional contour plot of the trispectrum is obtained by computing the amplitude of the trispectrum in the region of symmetry, $f_1 = c \geq 0$, $f_2$, $f_3 < 1$ Hz. This is illustrated in Figs. 10(b) and 11(b) that show a slice of the trispectrum.

[2]For a stationary random process, $x(k)$, the bispectrum is defined as $B(\omega_1,\omega_2) = E[X(\omega_1)X(\omega_2)X^*(\omega_1+\omega_2)]$, where $E[.]$ is the expected value, and $X(\omega)$ is the DFT of $x(k)$ at the frequency $\omega$. Similarly, the trispectrum can be defined as $T(\omega_1,\omega_2,\omega_3) = E[X(\omega_1)X(\omega_2)X(\omega_3)X^*(\omega_1+\omega_2+\omega_3)]$ [9].

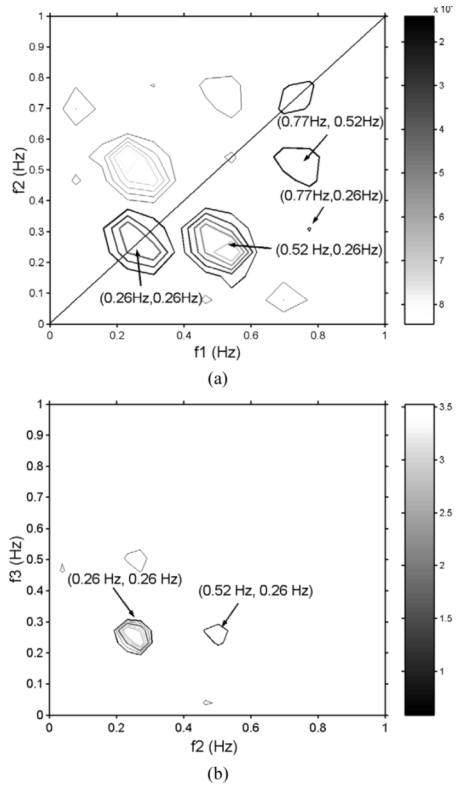


Fig. 10. Higher-order spectra of TEC-TOP signal. Case A. (a) Contour plot of the bispectrum. (b) Slice of trispectrum. Frequency window $f_1 \geq 0$, $f_2$, $f_3 \leq 1$ Hz.

Contour lines indicate the harmonic components interacting nonlinearly; the color bar in the plot provides a measure of the coupling strength; light shades represent low spectrum values, while dark shades indicate high spectral magnitude. As noted in [2] and [10], the amplitude of the bispectrum at the bifrequency $(\omega_1,\omega_2)$ measures the amount of coupling between the spectral components at the frequencies $\omega_1$, $\omega_2$, and $\omega_1 \pm \omega_2$. The components also have phases that are related at $\varphi_1$, $\varphi_2$, and $\varphi_1 \pm \varphi_2$ [i.e., the quadratically phase-coupled triplet $(\omega_1,\omega_2,(\omega_1+\omega_2)]$. Accordingly, the trispectrum is sensitive to the coupling between the spectral components at the frequencies $\omega_1$, $\omega_2$, $\omega_3$, and $\omega_1+\omega_2+\omega_3$ (cubically phase-coupled harmonics). If the phases are statistically independent of other components, the phases are random quantities, and the bispectrum (trispectrum) tends to zero. This enables to distinguish phase-coupled oscillations from unrelated oscillations.

Frequency modulation of the critical modes results in a nonlinear mechanism that is apparent in the HOS analysis in Figs. 10 and 11. As suggested from HSA, examination of these results confirms the presence of three- and four-wave modulation involving interarea modes 1 through 5. Thus, for instance, the analysis of bispectrum contours for the TEC-TOP signal in Fig. 10(a) shows self-interaction of the 0.26 Hz and frequency mixing at (0.52 Hz, 0.26 Hz). A minor interaction is also discernible between the 0.77-Hz mode and the 0.52-Hz mode and between the 0.77-Hz mode and the 0.26-Hz mode. Bispectral analysis of the MMT-JUI signal in Fig. 11(a), on the other hand, reveals the presence of a three-wave interaction between the 0.51- and the 0.32-Hz modes, the 0.76- and

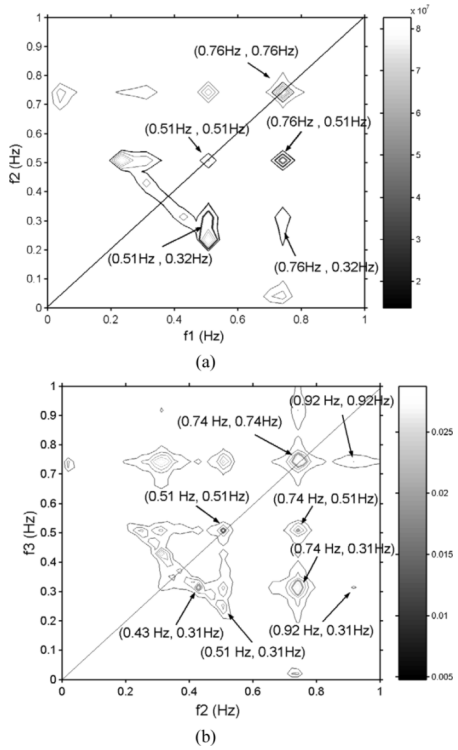


Fig. 11. Higher-order spectra of MMT-JUI 400-kV power flow signal. (a) Contour plot of the bispectrum. (b) Slice of trispectrum. Frequency window $f_1 \geq 0$, $f_2$, $f_3 \leq 1$ Hz.

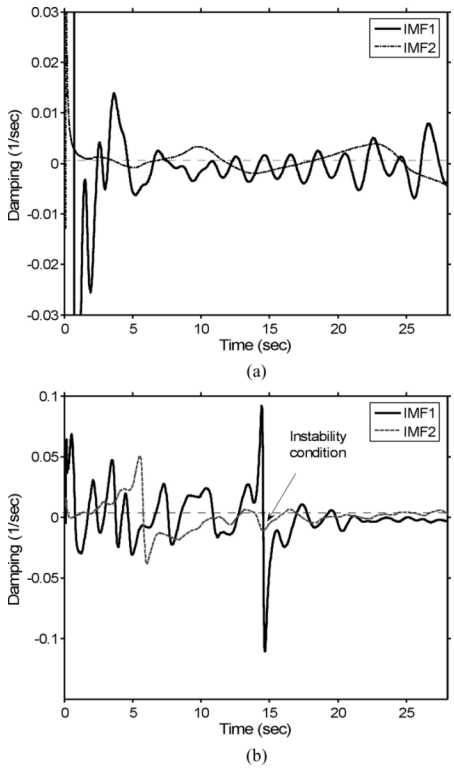


Fig. 12. Instantaneous damping of selected signals. (a) ALT-TMO signal. Case A. (b) TEC-TOP signal. Case A.

0.51-Hz modes, and between the 0.76- and 0.32-Hz modes. This is consistent with the Hilbert spectra shown in Fig. 6(b).

Analysis of the trispectrum for the TEC-TOP signal in Fig. 10(b) indicates, essentially, absence of cubic phase coupling. By contrast, the analysis of the trispectrum in Fig. 11(b) indicates a complex nonlinear relationship between the four slowest interarea modes. Components at $\omega_4 - \omega_1 = (0.76 \text{ Hz} - 0.31 \text{ Hz}) \approx (\omega_5 - \omega_2) = (0.92 \text{ Hz} - 0.51 \text{ Hz}) \approx 0.41$ Hz, along with a component at $(0.43 \text{ Hz} - 0.31 \text{ Hz}) \approx 0.12$ Hz are seen to occur due to cubic phase coupling between the frequency components in agreement with Hilbert results in Fig. 5(b). HOS analysis, however, provides no information about when the interactions generating the triplets occur in the time series.

### G. Damping Assessment via Hilbert Spectral Analysis

Further information about the nature of temporal behavior is obtained from the study of instantaneous damping. Using the procedure discussed in Section III-C, and assuming for simplicity that $\dot{\Lambda}_j(t)$ is a slowly varying function of time, the decay function for the $j$th IMF can be approximated by

$$\alpha_j(t) \approx -\frac{\dot{A}_j(t)}{A_j(t)}, \quad j = 1, \ldots p. \tag{8}$$

Fig. 12 shows the temporal variation of the decay factor of IMFs for selected signals computed using (8). Based on this computation, the time-varying system natural frequency and damping ratio and the local time-average of $\alpha_j(t)$ can be estimated.

TABLE II
PRONY ANALYSIS FIT. INPUT SIGNAL: ACTIVE POWER TEC-TOP 400-KV LINE

| Time window | Freq. (Hz) | Damping ratio | Relative amplitude |
|---|---|---|---|
| 1 | 0.4921 | -0.0073 | 0.359 |
| | 0.2630 | -0.0066 | 0.616 |
| | 0.7693 | 0.0164 | 1.000 |
| | 0.5269 | -0.0032 | 0.279 |
| 2 | 0.4921 | -0.0150 | 1.000 |
| | 0.2630 | -0.0066 | 0.773 |
| | 0.7595 | 0.0164 | 0.305 |
| | 0.5269 | -0.0032 | 0.155 |
| 3 | 0.4923 | -0.0146 | 1.000 |
| | 0.2612 | -0.0018 | 0.971 |
| | 0.7608 | 0.0158 | 0.277 |
| | 0.5267 | -0.0022 | 0.160 |

The analysis of the ALT-TMO and TEC-TOP interconnections confirms the onset of unstable oscillations. For the ALT-TMO signal, unstable oscillations are manifested by growing damping fluctuations with a negative mean value. For the TEC-TOP signal, instability for IMFs 1 and 2 is demonstrated at about 15 s and 5 s, as suggested from the analysis of the instantaneous amplitude in Fig. 5(a).

For comparison, Tables II–V show Prony results (PRS) for the selected time windows computed using [11]. Comparison of PRS of the original time series with those of IMF 1 for the TEC-TOP signal in Tables II and III shows that the first IMF is able to capture the essential system dynamics of the dominant modes, although some discrepancy is noted. In contrast, the

TABLE III
PRONY ANALYSIS FIT. INPUT SIGNAL: IMF 1, TEC-TOP 400-kV LINE

| Time window | Freq. (Hz) | Damping ratio | Relative amplitude |
|---|---|---|---|
| 1 | 0.4858 | -0.0209 | 0.529 |
| | 0.5255 | -0.0191 | 0.334 |
| | 0.7616 | 0.0173 | 1.000 |
| | 0.2247 | -0.0351 | 0.1221 |
| 2 | 0.4858 | -0.0209 | 0.529 |
| | 0.5255 | -0.0191 | 0.333 |
| | 0.7616 | 0.0173 | 1.000 |
| | 0.2247 | -0.0351 | 0.122 |
| 3 | 0.4999 | -0.0199 | 1.000 |
| | 0.1896 | 0.0916 | 0.222 |
| | 0.7632 | 0.0015 | 0.131 |

TABLE IV
PRONY ANALYSIS FIT. INPUT SIGNAL: MMT-JUI 400- kV LINE

| Time window | Freq. (Hz) | Damping ratio | Relative amplitude |
|---|---|---|---|
| 1 | 0.7431 | 0.0121 | 1.000 |
| | 0.5121 | 0.0134 | 0.364 |
| | 0.3144 | 0.0510 | 0.452 |
| | 0.9021 | 0.0607 | 0.302 |
| 2 | 0.7431 | 0.0120 | 1.000 |
| | 0.9058 | 0.0529 | 0.178 |
| | 0.3151 | 0.0486 | 0.169 |
| | 0.5117 | 0.0108 | 0.149 |

TABLE V
PRONY ANALYSIS FIT. INPUT SIGNAL: IMF 1, MMT-JUI 400- kV LINE

| Time window | Freq. (Hz) | Damping ratio | Relative amplitude |
|---|---|---|---|
| 1 | 0.7431 | 0.0121 | 1.000 |
| | 0.5117 | 0.0120 | 0.301 |
| | 0.9026 | 0.0542 | 0.280 |
| | 0.1421 | 0.8580 | 0.222 |
| 2 | 0.7430 | 0.0119 | 1.000 |
| | 0.5118 | 0.0108 | 0.438 |
| | 0.3144 | 0.0489 | 0.294 |
| | 0.8893 | 0.0581 | 0.031 |

comparison of Prony estimates for IMF1 of the MMT-JUI signal in Tables IV and V are shown to provide remarkable agreement with simulation results for the original time series for the three dominant modes at 0.74, 0.90, and 0.51 Hz. The results further confirm the validity of the procedures and point to the need for identifying precisely the operating conditions and time intervals for which conventional analysis may provide valid results.

## IV. CONCLUSIONS

Forced interarea oscillations resulting from critical contingencies may manifest highly complex phenomena, including second and higher modal interaction and non-stationary behavior. Using Hilbert analysis enables us to track the evolving dynamics of interaction mechanisms and identify the critical stages for analysis and control.

The study suggests that the time variability of the observed oscillations may be explained by quadratic and cubic nonlinear interaction between the frequency components. Quantitative information into the role and nature of the modal components involved in the transition to instability might be used to trigger control action to stabilize the system. In particular, the use of time-controlled discrete switching control actions and wide-area mode control based on the detection of critical stability damping margins of observed oscillations are being explored. The results are also relevant to the identification of the period of activity of critical modes.

## REFERENCES

[1] M. A. Andrade, A. R. Messina, C. S. Rivera, and D. Olguin, "Identification of instantaneous attributes of torsional shaft signals using the Hilbert transform," *IEEE Trans. Power Syst.*, vol. 19, no. 3, pp. 1422–1429, Aug. 2004.

[2] A. R. Messina and V. Vittal, "Assessment of nonlinear interaction between nonlinearly coupled modes using higher order spectra," *IEEE Trans. Power Syst.*, vol. 20, no. 1, pp. 1515–1521, Feb. 2005.

[3] S. Liu, A. R. Messina, and V. Vittal, "Characterization of nonlinear modal interaction using Hilbert analysis and normal form theory," in *Proc. IEEE Power Eng. Soc. Power Systems Conf. Expo.*, New York, Oct. 2004.

[4] J. J. Sanchez Gasca, V. Vittal, M. J. Gibbard, D. J. Vowles, S. Liu, and U. D. Annakage, "Analysis of higher order terms for small signal stability analysis," in *Proc. IEEE Power Eng. Soc. General Meeting*, San Francisco, CA, Jun. 2005.

[5] D. Ruiz Vega, A. R. Messina, and G. Harper, "Analysis of interarea oscillations via non-linear time series analysis techniques," in *Proc. 15th Power Systems Computation Conf.*, Liege, Belgium, Aug. 2005.

[6] N. E. Huang, Z. Shen, S. R. Long, M. C. Wu, H. H. Shih, Q. Zheng, N. C. Yen, C. C. Tung, and H. H. Liu, "The empirical mode decomposition and the Hilbert spectrum for nonlinear and non-stationary time series analysis," in *Proc. R. Soc. Lond. A*, 1998, vol. 454, pp. 903–995.

[7] R. R. Zhang, L. VanDemark, J. Liang, and Y. Hu, "On estimating site damping with soil nonlinearity from earthquake recordings," *Int. J. Nonlin. Mech.*, vol. 39, pp. 1501–1517, 2004.

[8] K. Worden and G. R. Tomlinson, *Nonlinearity in Structural Dynamics: Detection, Identification and Modelling*. Bristol, U.K.: IOP, 2001, p. 181.

[9] O. V. Pavlenko, "Nonlinear seismic effects in soils: numerical simulation and study," *Bull. Seismol. Soc. Amer.*, vol. 91, no. 2, pp. 381–396, 2001.

[10] C. L. Nikias and A. P. Petropulu, *Higher-Order Spectra Analysis—A Nonlinear Signal Processing Framework*. Englewood Cliffs, NJ: Prentice-Hall, 1993.

[11] J. M. Johnson and D. Trudnowski, BPA/PNNL Dynamic System Identification DSITools; Ringdown Analysis Tool. Columbus, OH, Batelle Memorial Institute, User's Manual, 1998.

**A. R. Messina** (M'85–SM'05) received the M.Sc. degree (Honors) in electrical engineering from the National Polytechnic Institute of Mexico, Mexico City, in 1987, and the Ph.D. degree from Imperial College, London, U.K., in 1991.

Since 1997, he has been a Professor at the Center for Research and Advanced Studies (Cinvestav), Mexico City. He is currently a Research Associate at Arizona State University, Tempe.

**Vijay Vittal** (M'82-SM'87-F'97) received the B.E. degree in electrical engineering from B.M.S. College of Engineering, Bangalore, India, in 1977, the M.Tech. degree from the Indian Institute of Technology, Kanpur, India, in 1979, and the Ph.D. degree from Iowa State University, Ames, in 1982.

He served on the faculty of the Department of Electrical and Computer Engineering at Iowa State University from 1982 to 2004. He is currently the Ira A. Fulton Chair of the Electrical Engineering Department, Arizona State University, Tempe.

Dr. Vittal received the 1985 Presidential Young Investigator Award and the 2000 IEEE Power Engineering Society Outstanding Power Engineering Educator Award. He is a member of the U.S. National Academy of Engineering.